# Shear Sensor for Lower Limb Prosthetic Applications

Kishore Sundara-Rajan, *Student Member, IEEE*, Gabriel I. Rowe, *Student Member, IEEE*, Anthony J. Simon, Glenn K. Klute, William R. Ledoux, and Alexander V. Mamishev, *Senior Member, IEEE*

***Abstract*—Lower limb amputees using a prosthetic device often suffer from mechanically-induced skin injuries. Shear stresses are believed to play a significant role in the formation of these skin injuries. The work presented in this paper is aimed at creating a new class of adaptive prosthetic and orthotic interfaces involving a capacitive shear stress sensor. The sensor design and transfer function are discussed. A few preliminary test results demonstrating the functionality of the sensor are also presented.**

## I. Introduction

IN the U.S., more than 180,000 people use an artificial leg or foot [1]. A large fraction of amputations are necessitated by complications of diabetes and atherosclerotic vascular disease. Skin irritation, ulcers, and tissue breakdown caused by mechanical loads prevent many lower extremity amputees from pursuing their vocational and recreational interests; discomfort is a common experience. This paper presents a capacitive sensor that is capable of measuring shear stresses; quantifying shear stress will increase our understanding of how friction blisters form and how to prevent them. The sensor presented here is a work in progress and this paper discusses the design process, transfer function, and preliminary bench tests.

## II. Sensing Technologies for Prostheses

The need for sensing at the skin-prosthesis interface has been long recognized. After the amputation of a portion of the lower limb, the leg undergoes changes including the muscular atrophy and volumetric conformation due to immune response and the use of a prosthetic device [2]. Friction blisters may form near bony protrusions and are normally treated by relieving pressure on that area with small foam or gel pads. Several groups worldwide are pursuing the design of technologies to resolve these issues. The common approach is to use a single mode sensor, such as pressure, and place it within the prosthetic socket at strategic locations. However, the spatial resolution or mechanical properties of any of the previously designed devices remains insufficient for adequate analysis of all variables of interest. An approach that would include the measurement of the primary variables involved in the formation of friction blisters (pressure, shear stress, temperature, and moisture), would provide researchers an unprecedented understanding of friction blister etiology. Devices for transduction of shear and pressure forces include resistive strain gauges [3], piezoelectric resistors [4], fiber-optic cables and waveguides, gas-filled cavities, and capacitance-based methods [5]. Since the established technologies rely upon rigid substrates such as silicon, very few sensors have been developed specifically to work within the prosthetic socket. One example where sensors were embedded into the socket lining was a foam-based shear sensor to monitor the effectiveness of the suction socket system [6]. Design of sensor pads in the field of robotics that are applicable to prosthetic socket analysis is a representative effort of a holistic approach to this problem.

The closest example of previous efforts to create sensors that combine the measurement of pressure and shear in one sensor is described in [7], and was used for tactile sensing on robotic finger tips. The advent of flexible electronics components and surface modification techniques developed in the last decade enables critical improvements to this general approach.

## III. Sensor Design

### A. Mechanical Design

We have developed a capacitive sensing based pressure and shear sensor. Two sets of electrodes (drive and sense) were patterned on printed circuit boards, and were encapsulated in polydimethylsiloxane (PDMS) layers. These layers were mechanically connected using 3 by 3 array of pillars also made from PDMS (Sylgard 184) (Fig. 1). The bottom layer of the sensor was anchored to a rigid base, and the top surface was exposed to the interfacial forces. When a shear stress was applied to the top surface of the sensor, the pillars bend along the direction of the force and, the top layer was displaced in the direction of the force.

The structural characteristics of the sensor, i.e., the stiffness when loaded, is determined by the diameter of the pillars and their height. A series of finite element simulations were conducted using the Comsol Multiphysics package to study the relationships between the lateral displacement of the top layer, applied force, structural stress in the sensor and the dimensions of the pillars. For these sets of simulations, a 3 by 3 equally spaced array of pillars was

Manuscript received March 13, 2009. This work was supported in part by the U.S. National Institute of Health under Grant R21HD052109-02 and the Department of Veterans Affairs Grant A4843C.

K. Sundara-Rajan, G. Rowe, A. J. Simon, and A. V. Mamishev are with the Sensors, Energy, and Automation Laboratory, Department of Electrical Engineering, University of Washington, Seattle, USA. (e-mail: kishore@u.washington.edu).

G. K. Klute, and W. R. Ledoux are with the Center of Excellence for Limb Loss Prevention and Prosthetic Engineering, VA Puget Sound Health Care System, Seattle, USA and the Department of Mechanical Engineering, University of Washington, Seattle, USA.

used. The top and bottom PDMS layers were each 2 mm thick, and had 2 cm sides. The finite element model (FEM) was meshed with 2994 nodes, resulting in a mesh of 12882 quadratic tetrahedral elements, with a minimum mesh quality of 0.1682. An isotropic linear elastic material model with Young's modulus of 868 kPa, Poisson ratio of 0.48, and density of 965 g/m$^3$ was used for the PDMS [8]. The linear elastic material model used in these simulations is valid only for small strains. In future iterations of this model, a non-linear hyperelastic material model will be used.

The relationship between the lateral displacement of the top electrode layer and the height and diameter of pillars was studied. A lateral force of 88 N (stress of 220 kPa) (after accounting for a safety factor of two for the forces reported in [9]) was applied along the x-axis and the height and the diameter of the pillars were varied from 1.5 mm to 3.0 mm (Fig. 2). Taller pillars had greater lateral displacement than shorter ones for the same force and the lateral displacement was inversely proportional to the diameter of the pillars. This behavior is in line with the analytical models [10].

The capacitance measurements have a higher signal to noise ratio and sensitivity when the electrode sets are placed close to each other, therefore making the shorter pillars desirable. The smaller lateral displacement of short pillars conflicts with the design parameters for the resolution of the sensor which is proportional to the lateral displacement. A minimum lateral displacement of about 0.7 mm was desired for the measurement system to have an adequate resolution of 0.088 N, and based on the lateral displacements predicted by finite element models (Fig. 2) a pillar of height 2.5 mm was selected.

To help in selection of the diameter of the pillars, the relationship between it and the maximum stress induced in the sensor structure for different pillar heights was studied (Fig. 3). When a lateral force is applied to the top surface, the pillars bend and they try to compress the bottom PDMS surface in addition to shearing them. Therefore the greatest stress occurs at the interface between the pillars and the bottom PDMS layer. The thinner pillars have less surface area to dissipate this force, and hence have higher stress levels than the thicker pillars.

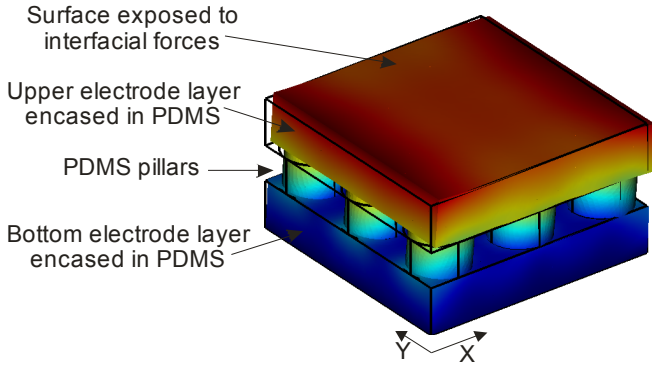


Fig. 1. 3D model of pressure and shear sensor. The shading of the model shows the displacement of the elements along the X-axis when the model is subjected to a lateral force of 88 N (stress of 220 kPa).

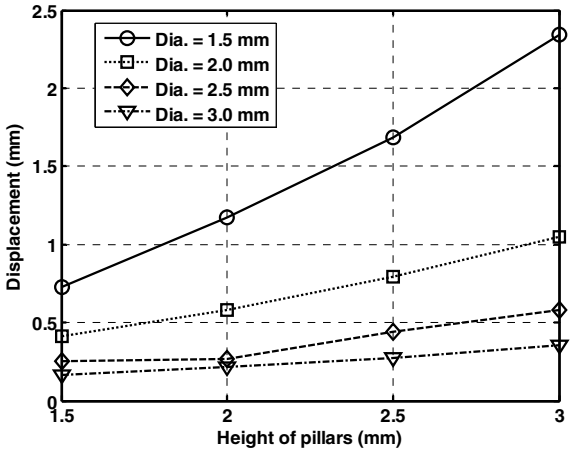


Fig. 2. Lateral displacement as predicted by finite element model of the top electrode layer when a lateral force of 88 N (stress of 220 kPa) is applied for the different structures with different pillar diameters and heights.

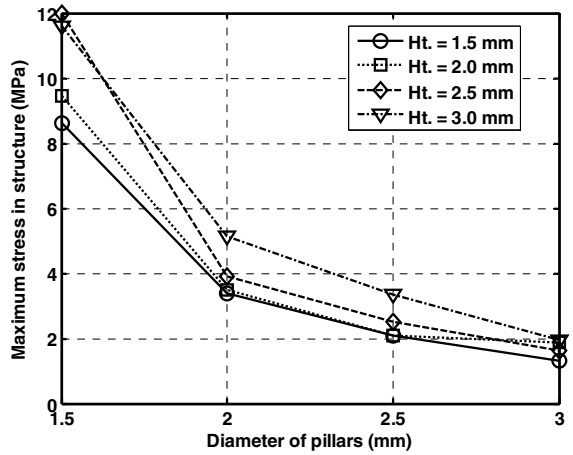


Fig. 3. The maximum stress in the structure when a lateral force of 88 N (stress of 220 kPa) is applied for different pillar diameters and heights as predicted by finite element models.

The structural models used for these simulations had an abrupt 90 degree transition between the pillar and the bottom PDMS layer. It was found that by filleting the ends of the pillars, the stress induced can be reduced by 61% (Fig. 4).

The diameter of the pillars needed to be so chosen such that it maximizes the lateral displacement while keeping the stress levels to a minimum. Another binding factor to consider is that the tensile or fracture strength of PDMS is 2.24 MPa [8]. Incorporating the 61% reduction in the predicted stress levels due to filleting of the pillars, the diameter chosen could not induce a stress greater than 3.6 MPa. Based on these limiting conditions, and the stress-diameter relationship predicted by finite element models (Fig. 3) a pillar diameter of 2 mm was chosen.

### *B. Electrical Design*

The sensor's electrode configuration is as follows: the drive electrodes ($D_1$, $D_2$, $D_3$, and $D_4$) are embedded in the rigid bottom PDMS layer and the sense electrodes ($S_1$, $S_2$,

$S_3$, and $S_4$) are embedded in the top layer (Fig. 5). The drive and sense electrode sets partially overlap with each other, thus forming 8 simple parallel plate capacitors ($C_1$-$C_8$). The electrodes are spatially positioned with respect to the PDMS pillars so that the effective dielectric permittivities of each of the 8 capacitances ($C_1$-$C_8$) are slightly different.

The effective capacitance between each electrode and ground with all other electrodes grounded ($C_{D1}$- $C_{D4}$, $C_{S1}$-$C_{S4}$) is measured. The measured capacitances can be approximated to be a linear combination of the overlap capacitances $C_1$-$C_8$ as shown in (1) where $\varepsilon_1$-$\varepsilon_8$ are offsets.

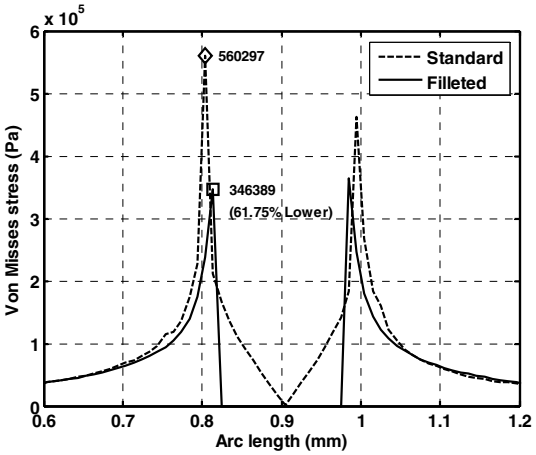


Fig. 4. Filleting the ends of the pillars reduces the stress induced at the interface between the pillars and the bottom PDMS layer by about 61%. The cross section was taken along the wall of the pillars going from the bottom of the pillar to the top, and the two peaks represent the bottom and top interfaces with the PDMS layers.

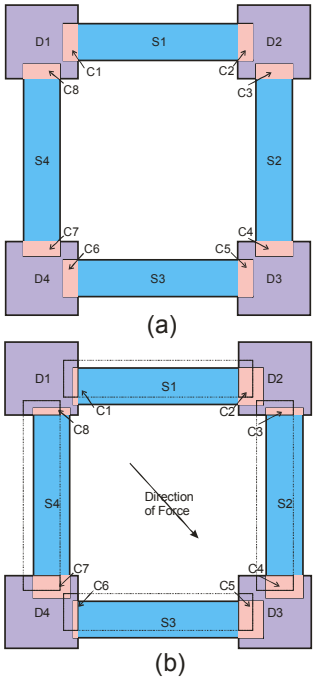


Fig. 5. (a)The drive electrodes ($D_1$, $D_2$, $D_3$, and $D_4$) are embedded in the rigid bottom PDMS layer and the sense electrodes ($S_1$, $S_2$, $S_3$, and $S_4$) are embedded in the top layer. (b) The area of overlap between these electrodes changes when a lateral force is applied, thus changing the trans-capacitance values.

$$\begin{aligned} C_{S1} &= C_1 + C_2 + \varepsilon_1 \\ C_{S2} &= C_3 + C_4 + \varepsilon_2 \\ C_{S3} &= C_5 + C_6 + \varepsilon_3 \\ C_{S4} &= C_7 + C_8 + \varepsilon_4 \\ C_{D1} &= C_1 + C_8 + \varepsilon_5 \\ C_{D2} &= C_2 + C_3 + \varepsilon_6 \\ C_{D3} &= C_4 + C_5 + \varepsilon_7 \\ C_{D4} &= C_6 + C_7 + \varepsilon_8 \end{aligned} \tag{1}$$

When a shearing force is applied, the pillar array bends and compresses. This changes the area of overlap between the drive and sense electrodes as shown in Fig. 5(b). The change in the measured capacitances ($C_{D1}$- $C_{D4}$, $C_{S1}$- $C_{S4}$) are a composite of change in areas of overlap along the $x$ and $y$ directions, as well as displacement along the $z$ direction due to any normal load. To isolate these effects, we consider variations of the trans-capacitances ($\Delta C_1$-$\Delta C_8$). The relationship between the electrode displacements, $\Delta x$, $\Delta y$, and $\Delta z$ along the Cartesian coordinates and the variations in the trans-capacitances is given by (2) where $p$, $n_1$-$n_8$, and $l_1$-$l_8$ are linear coefficients that are dependent on the areas of overlap.

$$\begin{bmatrix} \Delta C_1 \\ \Delta C_2 \\ \Delta C_3 \\ \Delta C_4 \\ \Delta C_5 \\ \Delta C_6 \\ \Delta C_7 \\ \Delta C_8 \end{bmatrix} = \frac{p}{\Delta z} \begin{bmatrix} -1 & n_1 \\ 1 & n_2 \\ 0 & n_3 \\ 0 & n_4 \\ 1 & n_5 \\ -1 & n_6 \\ 0 & n_7 \\ 0 & n_8 \end{bmatrix} \Delta x + \begin{bmatrix} 0 & l_1 \\ 0 & l_2 \\ 1 & l_3 \\ -1 & l_4 \\ 0 & l_5 \\ 0 & l_6 \\ 1 & l_7 \\ -1 & l_8 \end{bmatrix} \Delta y \tag{2}$$

### C. *Inverse Problem*

To estimate the shear stress based on the measurements made, the following procedure is adopted.

By simple algebraic manipulation of (1), the variation in elemental capacitances $\Delta C_1$-$\Delta C_8$ can be calculated from the changes in measured values as shown in (**3**) where $m_{11}$-$m_{88}$ are the linear coefficients and $k_1$-$k_8$ are the offsets.

$$\begin{bmatrix} \Delta C_1 \\ \Delta C_2 \\ \cdots \\ \Delta C_7 \\ \Delta C_8 \end{bmatrix} = \begin{bmatrix} m_{11} & m_{12} & \cdots & m_{18} \\ m_{21} & \cdots & & \\ \cdots & & \cdots & \\ m_{81} & & & m_{88} \end{bmatrix} \begin{bmatrix} \Delta C_{S1} \\ \Delta C_{S2} \\ \cdots \\ \Delta C_{D3} \\ \Delta C_{D4} \end{bmatrix} + \begin{bmatrix} k_1 \\ k_2 \\ \cdots \\ k_7 \\ k_8 \end{bmatrix} \tag{3}$$

Since the net change in areas of overlap when all the trans-capacitances are considered is zero, the net change in elemental capacitances is due to the change in the distance between the electrodes, $\Delta z$. Therefore,

$$\Delta z = a\sum_{i=1}^{8}\Delta C_i \tag{4}$$

where, $a$ is a linear co-efficient that is dependent on the effective dielectric constant between the electrodes. Once $\Delta z$ is known, the lateral displacements $\Delta x$, and $\Delta y$ can be determined by taking ratios of the change in elemental capacitances and accounting for changes due to normal displacement, as shown in (5).

$$\begin{aligned}\Delta x &= \frac{\Delta C_2}{\Delta C_1} - g(\Delta z) = \frac{\Delta C_5}{\Delta C_6} - g(\Delta z)\\ \Delta y &= \frac{\Delta C_3}{\Delta C_4} - h(\Delta z) = \frac{\Delta C_8}{\Delta C_7} - h(\Delta z)\end{aligned} \tag{5}$$

where, $g(\Delta z)$ and $h(\Delta z)$ are functions that compensate for variations in the capacitances due to normal displacements. The exact nature of these functions is complex and is discussed in detail in [11]. At the time of this publication, the exact nature of $g(\Delta z)$ and $h(\Delta z)$ for this sensor has not been determined and hence the results presented in the next section do not compensate for the vertical movements. Since the effective dielectric permittivity of each of the elemental capacitances is slightly different, the ratio of the capacitances is a measure of the displacements. The mapping between the displacement and the shearing force will be obtained by calibration based techniques.

## IV. Experimental Data

To conduct bench based performance tests of the sensor, the bottom of sensor was attached to a rigid surface, and the top electrode was displaced by known distances using LabView controlled Newport precision stages. Capacitance measurements were made using the using a Cypress Semiconductor CY8C21434 mixed signal IC based circuitry.

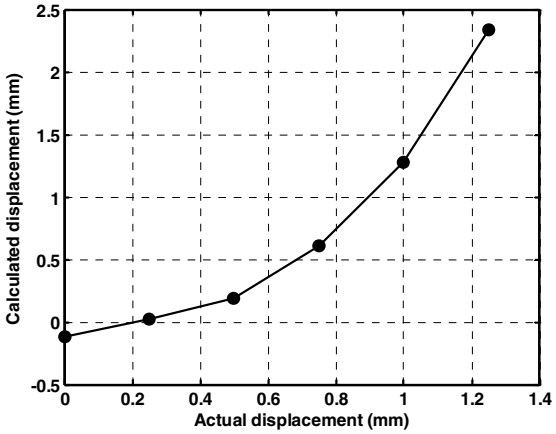


Fig. 6. The calculated lateral displacement is a cubic function of the actual lateral displacement. This is due to the top electrode being displaced in the normal direction when the pillars bend.

To simplify the setup, there was no normal pressure applied to the sensor. Fig. 6 shows the relationship between the calculated lateral displacement and the actual lateral displacement of the sensor. The calculated lateral displacement is nearly a cubic function of the actual lateral displacement. This is due to the vertical displacement of the electrodes when the pillars bend from the lateral forces. When the electrodes move closer to each other, the effective capacitance between them increases nearly exponentially [11]. This component of the normal displacement has not been accounted for in the model and will be included in future iterations.

## V. Conclusion and Future Work

A capacitance based shear sensor was designed, fabricated, and shown to be functional. A simple transfer function was developed and tested. As a next step, the transfer function will be expanded to accommodate for normal displacements due to the bending of pillars. The transfer function method will be replaced with a simple calibration based one once the sensors have been tested and mechanically characterized.

## References


[1] "Statistical Abstract of the United States," United States Bureau of the Census, 1995.

[2] Z. Ming, A. F. T. Mak, A. I. K. Chung, and K. H. Chung, "MRI Investigation of Musculoskeletal Action of Transfemoral Residual Limb Inside a Prosthetic Socket," *Proceedings of the 20th Annual International Conference of the IEEE Engineering in Medicine and Biology Society*, vol. 5, 1998, pp. 2741-2743.

[3] J. Engel, J. Chen, C. Liu, B. R. Flachsbart, J. C. Selby, and M. A. Shannon, "Development of Polyimide-Based Flexible Tactile Sensing Skin," *Materials Research Society Symposium*, vol. 736, 2003, pp. D4.5.2-D4.5.6.

[4] C. Domenici, D. De Rossi, A. Bacci, and S. Bennati, "Shear Stress Detection in an Elastic Layer by a Piezoelectric Polymer Tactile Sensor," *IEEE Transactions on Dielectrics and Electrical Insulation*, vol. 24, no. 6, pp. 1077-1081, 1989.

[5] T. R. Filanc-Bowen, H. K. Geun, and Y. M. Shkel, "Novel Sensor Technology for Shear and Normal Strain Detection With Generalized Electrostriction," *Proceedings of IEEE Sensors*, vol. 2, 2002, pp. 1648-1653.

[6] C. Glass, M. Bain, and W. Craelius, "Interface Monitoring of a Prosthetic Silicone Suction Socket System," *IEEE Twenty-Second Annual Northeast Bioengineering Conference*, 1996, pp. 82-83.

[7] T. A. Chase and R. C. Luo, "A Thin-Film Flexible Capacitive Tactile Normal/Shear Force Array Sensor," Proceedings of the 21st IEEE International Conference on Industrial Electronics, Control, and Instrumentation, vol. 2, 1995, pp. 1196-1201.

[8] J. E. Mark, *Polymer data handbook,* Oxford University Press., 1999.

[9] M. Yavuz, A. Tajaddini, G. Botek, and B. L. Davis, "Temporal Characteristics of Plantar Shear Distribution: Relevance to Diabetic Patients," *Journal of Biomechanics*, vol. 41, no. 3, pp. 556-559, 2008.

[10] C. Mohrdieck, A. Wanner, W. Roos, A. Roth, E. Sackmann, J. P. Spatz, and E. Arzt, "A Theoretical Description of Elastic Pillar Substrates in Biophysical Experiments," *Chemphyschem*, vol. 6, no. 8, pp. 1492-1498, Aug. 2005.

[11] G. I. Rowe and A. V. Mamishev, "Simulation of a Sensor Array for Multiparameter Measurements at the Prosthetic Limb Interface," Health Monitoring and Smart Nondestructive Evaluation of Structural and Biological Systems III, vol. 5394, 7-21-2004, pp. 493-500.